Scaling properties and anomalous diffusion of the Florina micro-seismic activity: Fluid driven?

Georgios Michas [a,*], Filippos Vallianatos [a,b]

[a] UNESCO Chair on Solid Earth Physics and Geohazards Risk Reduction, Hellenic Mediterranean University, Crete, Greece
[b] Department of Geophysics–Geothermics, Faculty of Geology and Geoenvironment, National and Kapodistrian University of Athens, Athens, Greece

ARTICLE INFO

ABSTRACT

Episodic earthquake activity associated with pore-fluid pressure diffusion in the crust can frequently be observed in intraplate regions, particularly related with past volcanism. Increased micro-seismicity has been observed during 2012–2014 in such an area, near the CO_2-rich Florina basin (North Greece). Using a high-resolution relocated catalog for the area, we use concepts of statistical physics to study the spatiotemporal and diffusion properties of micro-seismicity and investigate the possible involvement of fluids in the triggering mechanism. The spatial distribution of events shows that seismicity mainly occurred in two clusters, one dipping to the north (cluster A) and the other on an almost vertical fault plane (cluster B). We focus on cluster B, which was mainly activated after the installation of a local seismic network, able to detect and record the increased micro-seismicity in the area. Cluster B was activated during two main periods (periods B1–B2), with an almost vertical alignment of events with depth. During the second period of activation (period B2), events are migrating towards the surface with time indicating a diffusive process. Furthermore, the estimation of the mean square displacement of seismicity with time during the two main periods of activation shows very weak earthquake diffusion during period B1, but more pronounce earthquake diffusion during period B2, with a diffusion exponent that corresponds to a sub-diffusive process. In addition, we use non-extensive statistical mechanics to study the spatiotemporal scaling properties of seismicity, with results that indicate correlated behavior and organization patterns during both periods of activation. Observations and analysis indicate the possible involvement of fluids in the triggering mechanism of micro-seismicity. However, continued monitoring of seismicity and CO_2 discharging would be required to better constrain the relation between seismicity and CO_2 emissions in the CO_2-rich Florina basin and to better quantify the associated earthquake and environmental hazards.

1. Introduction

Episodic earthquake activity, associated with magmatic intrusions and/or fluid migration and pore-pressure perturbations in the crust, is frequently observed in volcanic areas,[1] but also in intraplate regions, particularly associated with past volcanism, such as the Vogtland/NW Bohemia region[2] and the Long Valley caldera/Mammoth Mountain, California.[3] In such intraplate regions, the interplay between the regional tectonic stresses and the presence of highly pressurized fluids, released from volatiles like CO_2, can be the triggering mechanism of episodic earthquake activity, which often presents the characteristics of earthquake swarms, described by the occurrence of numerous small earthquakes strongly clustered in time and space and the absence of

any dominant mainshock and the typical mainshock–aftershock sequence frequently observed in tectonic earthquakes.[4]

The diffusion of pressurized CO_2-rich fluids has been proposed to explain the occurrence of earthquake swarms in the Mammoth Mountain[3,6] and the Vogtland/NW Bohemia,[2,7] whereas the co-seismic release and diffusion of trapped CO_2 has been proposed as the triggering mechanism of the 1997 Umbria-Marche (North Italy) episodic earthquake sequence.[8] A characteristic feature in these cases is the migration of seismicity, which is thought to reflect fluid migration or pore-pressure diffusion occurring preferentially along faults, fractures and zones of weakness that act as permeable channels for fluids to flow.[9] According to the Coulomb failure criterion, a pore-pressure increase due to the presence of pressurized fluids, or pore-pressure perturbations in an already pressurized system, can decrease the effective normal stress along critically stressed fractures and faults, triggering earthquakes. In addition, the circulation of hydrothermal fluids

* Corresponding author.
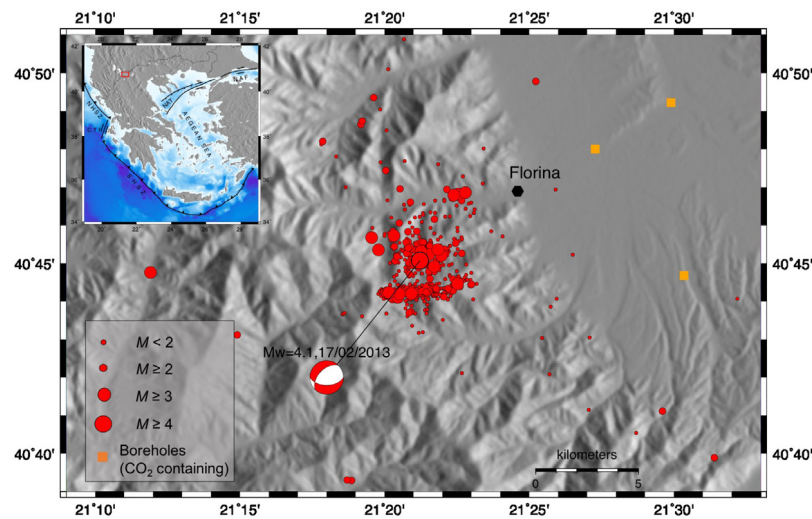*E-mail address:* gmichas@hotmail.com (G. Michas).

Fig. 1. Epicentral map of the 2012–2014 micro-seismic activity (circles) in the area of Florina. The main CO_2-containing boreholes in the Florina Basin are shown with squares. The relocated epicenters and the focal mechanism of the M_w4.1 earthquake is after.[5] Inset: The broader area of Greece and the main tectonic setting (SHSZ: South Hellenic Subduction Zone, NHSZ: North Hellenic Subduction Zone, KTF: Cephalonia Transform Fault, NAF: North Anatolian Fault, NAT: North Aegean Trough). The rectangle indicates the study area.

in the crust may act as an additional weakening effect due to hydrothermal alterations, which can further reduce the friction coefficient and the Coulomb failure criterion.[10]

In 2012–2014 increased micro-seismicity occurred near the city of Florina (North Greece).[5] The Florina basin is the main commercial exploitation site of CO_2 in Greece. Carbonate rich springs and CO_2-rich gas vents are observed throughout the Florina Basin as the outcome of slow upwelling of deep origin magmatic-hydrothermal CO_2 through the regional fracture and fault network.[11] Gas manifestations mainly originate from crustal sources, with an additional minor ($\sim$10%) mantle contribution and are probably related to Quaternary volcanism.[12] In addition, mineral springs and gas bubbles in shallow wells due to localized CO_2 leakages are aligned in a general NE–SW direction, parallel to one of the main regional fault directions, further supporting the important role of the regional fractures and faults in CO_2 migration and upwelling.[13] The importance of the area is further enhanced by its consideration as a possible CO_2 geological storage site.[14]

The increased micro-seismicity in the area of Florina has previously been described by Mesimeri et al.[5] In the latter study,[5] the concept of seismicity triggering fronts in a homogeneous and isotropic medium, e.g. Ref. 9, was used as a first approximation for investigating the possible involvement of fluid diffusion in the triggering mechanism of micro-seismicity in the area. In the present work we use a different approach, based on concepts of statistical physics and complexity theory, to study the spatiotemporal scaling and diffusion properties of the micro-seismic activity in the area of Florina, where "diffusion" is used as a generic term to denote the spatial migration of seismicity. The main objective is to better understand the physical characteristics of micro-seismicity and to investigate its possible connection to CO_2 migration. Such studies are fundamental for understanding the CO_2 migration mechanisms and for better quantifying earthquake and environmental hazards, particularly in sites that are considered as natural analogues for carbon geological storage.

2. The Florina micro-seismic activity

Earthquake activity in Northern Greece and particularly in the area of Florina can be considered moderate, as both historic and instrumental records indicate only 5 earthquakes of magnitude

$5 \leq M \leq 6$ in the broader area, with the largest being the 1709 M6 earthquake that occurred at about 20 km SW from the city.[15] In July 2012 micro-seismic activity ($M \leq 3.5$) started to occur just SW of the city of Florina (Fig. 1).[5] The earthquake activity in the broader area is continuously being recorded by the Hellenic Unified Seismological Network (HUSN). However, the sparse distribution of the network in Northern Greece and its low detectability in low magnitude earthquakes are not adequate to detect micro-seismicity. To efficiently record the increased micro-seismicity in the area, a local network comprised of six broadband seismometers was installed at the end of July 2013 by the Geophysics Department of the Aristotle University of Thessaloniki. During the 6-months operation period, approximately 1500 earthquakes were detected by the local network. Using a novel velocity model for the area, Mesimeri et al.[5] relocated the earthquakes recorded from both the local and the permanent (HUSN) network, resulting in a relocated catalog comprising of 1753 earthquakes, available at http://geophysics.geo.auth.gr/ss/station_index_en.html. The horizontal and vertical errors of the relocated earthquakes range between 2 m and 35 m, with a magnitude of completeness $Mc = 1.3$ for the relocated catalog.[5]

The spatial distribution of the relocated earthquakes in the vicinity of Florina is shown in Fig. 1. Micro-seismicity is mainly distributed in two clusters, one in the north that includes the largest event of the sequence (M_w4.1) occurred on February 17, 2013 and the other in the south, having an almost E–W general direction (Fig. 1). The majority of events on the northern cluster, which we name cluster A, occurred at depths $\sim$4 – 6 km on a fault segment dipping at $\sim$45° to the north (see Ref. 5), in accordance to the focal mechanism of the M_w4.1 event. The southern cluster, which we name cluster B, was mainly activated after the 29th July 2013. The majority of seismic events occurred on an almost vertical fault plane gently dipping to the south at shallow depths between 2 and 4.5 km (see Fig. 2 and the discussion in Ref. 5).

The spatiotemporal evolution of the entire sequence was thoroughly described in Ref. 5. In the present study we focus only on cluster B that was mainly activated after the installation of the local network. Cluster B counts 540 earthquakes for $M \geq Mc$ and for the period between 29/07/13 and 12/01/14. Fig. 2 shows the temporal evolution of seismicity along cluster B with depth (see also Fig. 5b in Ref. 5). From Fig. 2 we can distinguish three basic features. The first is that seismicity mainly occurred at depths
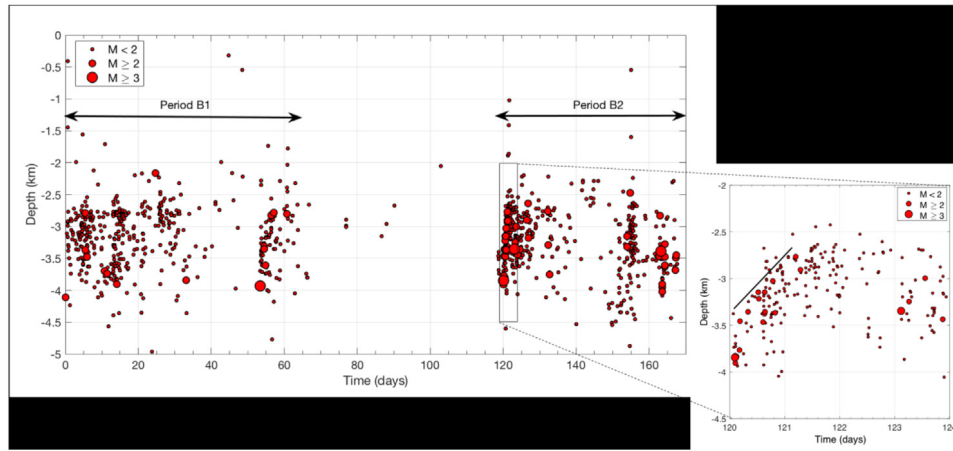
Fig. 2. Temporal evolution of seismicity on cluster B with depth (see also Fig. 5b in Ref. 5). On the *x*-axis, time is counted in days since the 29th July, 2013. On the right image, the solid line indicates the spatial migration of seismicity towards shallower depths.

between 2 and 4.5 km. The second is that we can distinguish two main periods of activation, the first starting with an episodic increase of seismicity on 29th July 2013, lasting approximately 66 days (period B1; Fig. 2). After a quiescent period between October-04 and November-24 2013, another significant increase of seismicity occurred on 24 November 2013 that lasted for almost 49 days (period B2; Fig. 2), till mid-January 2014 (see also the discussion in Ref. 5). The third feature is the spatial migration of seismicity towards shallower depths at approximately 0.6 km/day, observed during the first three days of period B2 (Fig. 2), which may indicate the possible involvement of CO_2-rich fluids that are diffusing at negative pressure gradients towards the surface, in the triggering mechanism of seismicity along cluster B.

3. Scaling properties and diffusion of the micro-seismic activity

We further study the scaling and diffusion properties of micro-seismicity that occurred on cluster B after the end of July 2013. We focus our analysis on cluster B and the selected time period mainly due to the installation of the local network during that period that offers a more complete image in the evolution of micro-seismicity, but also because it offers the opportunity to study the properties of micro-seismicity on a single activated structure. The spatiotemporal scaling properties of seismicity can provide important information regarding the structure and the underlying processes of seismicity, while an active earthquake diffusion mechanism may be indicative for fluid involvement in the triggering mechanism of seismicity.

3.1. Scaling properties of micro-seismicity

In the previous section we saw that cluster B was mainly activated during 2 main periods (Fig. 2), the first between 29/07/2013 – 03/10/2013 (period B1) and the second between 24/11/2013 – 12/01/2014 (period B2). We analyze the spatiotemporal scaling properties during the two distinct periods of activity for earthquakes with $M \geq Mc$ to investigate possible organization and clustering patterns in the evolution of seismicity.

To perform such an analysis, we consider earthquake activity as a point-process in time and space, marked by the magnitude of the event. To study the spatiotemporal scaling properties, we estimate the cumulative distributions $P(>\tau)$ of inter-event times τ and $P(>r)$ of inter-event distances r between the successive earthquakes, where τ and r are given by $\tau = t_{i+1} - t_i$ and

$r = \|x_{i+1} - x_i\|$, with i = 1, 2, ..., $N - 1$ (N the total number of events) and t, x are the time of occurrence and the location (hypocenter) of the events, respectively. In the case that we study here that includes only a few hundreds of events, the cumulative distribution is preferred to the probability density, as it assimilates the entire dataset without making assumptions about the binning intervals, thus producing smoother and unbiased trends in the observed distributions.

Rather than using simple statistical models to study the spatiotemporal scaling behavior of micro-seismicity, we incorporate in the analysis the notions of statistical physics and the maximum entropy principle[16] to infer the least biased probability distribution that can describe the observed scaling behavior. Considering possible correlations in the evolution of seismicity, we optimize the non-additive entropy S_q introduced by Tsallis in the framework of non-extensive statistical mechanics.[17,18] The non-additive entropy S_q incorporates properties such as (multi)fractal structures and long-range correlations, properties that are intrinsic characteristics of seismicity.[19-23] For a continuous variable X the non-additive entropy S_q is given by Ref. 18:

$$S_q = k \frac{1 - \int_0^\infty p^q(X)dX}{q - 1}, \tag{1}$$

where k is a positive constant, such as Boltzmann's constant and $p(X)$ ($0 \leq p(X) \leq 1$) the probability distribution of X. By optimizing S_q, given the appropriate constraints (see Refs. 18, 21), we derive the following cumulative distribution function, commonly known in the literature as the q-exponential distribution[18]:

$$P(> X) = \left[1 - (1 - q)\frac{X}{X_0}\right]^{\frac{2-q}{1-q}}, \tag{2}$$

where X_0 and q are positive scaling parameters. Note that the cumulative distribution function given in Eq. (2) is a particular case that maximizes S_q by integrating the physical probability $p(X)$ instead of the escort probability $p_q(X)$ in the second constraint and the condition of the mean value, although the various forms of the derived q-exponential functions are similar (see Refs. 18, 21 for the analytic derivation and discussion of Eq. (2)). In this case, the inverse of the q-exponential (Eq. (2)) is the q-logarithmic distribution, defined as:

$$\ln_{q'}(X) = \frac{[P(> X)]^{1-q'} - 1}{1 - q'}, \tag{3}$$

with $q' = 1/(2 - q)$.[24] After the estimation of the appropriate q-value that best describes the distribution of X, the q-logarithmic

distribution (Eq. (3)) is, according to theory, linear with X,[25] so that it can be used as a goodness-of-fit test between the data and the model.

In the limit of $q \to 1$, S_q precisely recovers the standard Boltzmann–Gibbs entropy S_{BG}, while the q-exponential and the q-logarithmic, the exponential and logarithmic distributions, respectively. For $q > 1$, the q-exponential distribution exhibits asymptotic power-law behavior, while for $q < 1$ a cut-off appears.[26] Hence, the q-parameter indicates how far or close to the exponential and thus to random (Poissonian) behavior the distribution is. The present approach thus offers a unified framework that produces a range of distributions, varying from power-law to exponential, which are both ubiquitous in nature.[26]

The q-exponential distribution has found wide applications in the statistical physics of earthquakes, for a variety of regional scales and tectonic environments, signifying the importance of asymptotic power-law behavior and long-range correlations in the earthquake generation process.[18,21,23,26–34] In addition, the q-exponential distribution appears quite stable in missing events from the dataset, thus producing more robust results.[27] In the following, we use the q-exponential distribution (Eq. (2)) to approximate the observed scaling behavior of $P(>\tau)$ and $P(>r)$ and the q-logarithmic distribution (Eq. (3)) as a goodness-of-fit test between the data and the model. We estimate the model parameters with the Levenberg–Marquardt nonlinear least squares algorithm, while the associated 95% confidence intervals were calculated from the covariance matrix of the estimated parameters (e.g. Ref. 35). To further enhance confidence on the results, we use an additional goodness-of-fit test, the Kolmogorov–Smirnov test, to test the null hypothesis that the dataset comes from the q-exponential distribution.

Fig. 3 shows the observed cumulative distributions $P(>\tau)$ of the inter-event times τ for the two distinct periods of activity (periods B1–B2) along cluster B, as well as the q-exponential distribution fitted to the data. For period B1, the q-exponential distribution describes well the observed scaling behavior and particularly the broad tail of the distribution, for the values of $q_\tau = 1.46 \pm 0.02$ and $\tau_0 = 0.061 \pm 0.004$ days. Similarly, for period B2, the q-exponential distribution describes well the observed $P(>\tau)$ for the values of $q_\tau = 1.53 \pm 0.023$ and $\tau_0 = 0.016 \pm 0.0015$ days and up to a characteristic time $\tau_c \approx 0.8$ days, where a fall-off in the distribution appears (Fig. 3b), probably due to the finite size of the sequence that ended at mid-January 2014, limiting the occurrence of sporadic events and hence the emergence of long inter-event times (finite-size effect). The much higher than unity q_τ-value indicates asymptotic power-law behavior and long-range correlations in the temporal evolution of seismicity, with similar q_τ-values for the two time periods. In the insets of Fig. 3a and b, the corresponding q-logarithmic distributions are shown that approximate linearity with the high correlation coefficients of 0.991 and 0.997 (for τ up to 0.8 days) for periods B1 and B2, respectively, further supporting the goodness-of-fit between the model and the data. In addition, the Kolmogorov–Smirnov test does not reject the null hypothesis that the data come from the q-exponential distribution at the 1% significance level (test statistic 0.1076, p-value 0.021 and critical value 0.116 for period B1; test statistic 0.0772, p-value 0.0314 and critical value 0.0872 for period B2), further enhancing confidence on the fitting results.

Furthermore, we study the scaling properties of the inter-event distances r between the successive earthquakes for periods B1 and B2. Fig. 4 shows the observed cumulative distributions $P(>r)$ for the two time periods and the corresponding fit according to the q-exponential distribution (Eq. (2)). In this case, the q-exponential distribution describes well the observed distributions for q_r-values less than unity and particularly for the values

of $q_r = 0.87 \pm 0.03$ and $r_0 = 1.13 \pm 0.024$ km for period B1 and $q_r = 0.75 \pm 0.027$ and $r_0 = 1.215 \pm 0.022$ km for period B2, respectively. As for the inter-event times, the inter-event distances of the micro-seismic activity deviate from the exponential function, indicating organization rather than random spatial occurrence along the active fault structure. The corresponding q-logarithmic distributions approximate linearity with the high correlation coefficients of 0.998 and 0.992 for periods B1 (Fig. 4a) and B2 (Fig. 4b), respectively, indicating the goodness-of-fit between the model and the data. Failure on rejecting the null hypothesis at the 1% significance level by the Kolmogorov–Smirnov test further enhances confidence on the fitting results (test statistic 0.0492, p-value 0.716 and critical value 0.116 for period B1; test statistic 0.074, p-value 0.0445 and critical value 0.0873 for period B2).

3.2. Diffusion properties

In the case where fluid diffusion is involved in the triggering mechanism of micro-seismicity in the area, we may expect to see some signs of earthquake migration in the evolution of the sequence.[9] Earthquake migration in this case can be related to fluid diffusion and the migration of CO_2-rich fluids, which, according to the Coulomb failure criterion, can reduce the effective normal stress along the fault plane triggering earthquakes. As a first approximation, some evidence for an active diffusion mechanism can be provided by the almost vertical alignment of seismicity along the fault structure during both periods B1 and B2, as well as the migration of seismicity towards shallower depths at the beginning of period B2 (Fig. 2).

To quantify earthquake diffusion, we use notions of the random walk theory to estimate the mean square displacement (msd) of seismicity with time.[36] The msd is estimated relevant to some reference point, which we consider it to be the first event during periods B1 and B2, respectively. We calculate the 3D Euclidean distance x of each event from the reference (1st event) for the two periods and then estimate the mean square displacement (msd) as:

$$\langle x^2(t) \rangle = \frac{1}{N} \sum_{n=1}^{N} x_n^2(t), \tag{4}$$

where N is the total number of events and $x_n(t)$ is the distance of the nth earthquake from the reference at time t. In this way we can calculate the average expansion of seismicity in respect to the first event (reference point) of the sequence and then make inferences about the diffusion process itself. An increasing msd indicates migration of seismicity away from the reference, a decreasing msd indicates that seismicity is moving closer to the reference and a constant msd indicates no migration of seismicity in respect to the reference.

Of particular importance is the function of the msd with time. In normal diffusion (Brownian motion), the msd is linearly dependent on time. However, in complex heterogeneous media other functions are encountered that frequently take the form of a power-law[37]:

$$\langle x^2(t) \rangle \sim t^a. \tag{5}$$

In the last equation the diffusion exponent a characterizes the different diffusion regimes. In a homogeneous and isotropic medium, normal, or "homogeneous" diffusion is expected. In this case, the msd is linearly dependent on t ($a = 1$). Instead, the hallmark of anomalous ("nonhomogeneous") diffusion in complex heterogeneous media is the non-linear growth of the msd with time.[37] In this case and for $a > 1$ the diffusion process is super-diffusive, while for $0 < a < 1$ it is sub-diffusive.
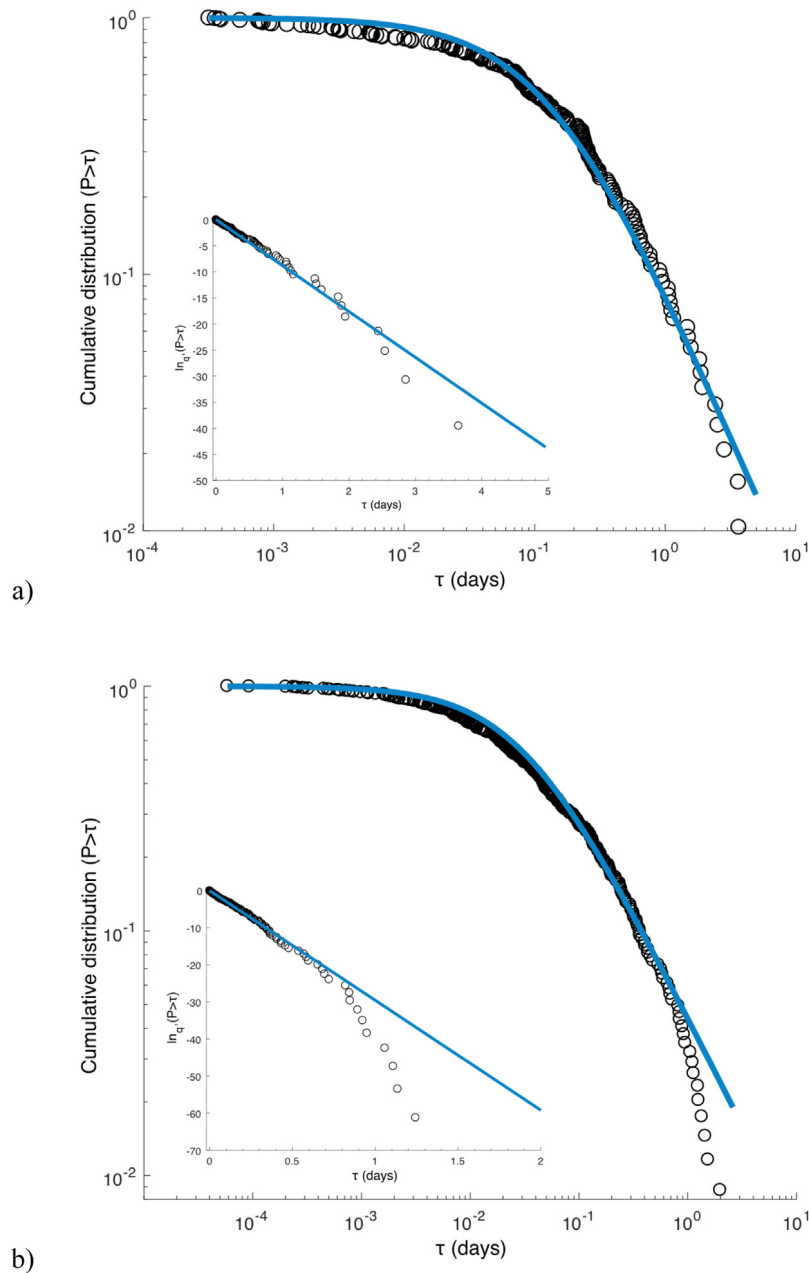
Fig. 3. (a) Cumulative distribution function $P(>\tau)$ for period B1 and the corresponding fit according to the q-exponential distribution (Eq. (2)) for the values of $q_\tau = 1.46$ and $\tau_0 = 0.061$ (solid line). Inset: the corresponding q-logarithmic distribution that approximates linearity with the correlation coefficient of -0.9912. (b) The same for period B2. The q-exponential distribution (solid line) takes the values of $q_\tau = 1.53$ and $\tau_0 = 0.016$, while the q-logarithmic distribution (inset) approximates linearity with the correlation coefficient of -0.997 for τ up to 0.8 days and -0.9791 for the entire period.

This approach has been used as a statistical measure for the rate of earthquake diffusion and the spatial expansion of seismicity in aftershock sequences, regional seismicity and fluid-related earthquake swarms.[36,38–40] In all these studies it has been shown that earthquake diffusion generally follows a power-law growth with time (Eq. (5)), with power-law (or "diffusion") exponents much lower than unity, indicating the sub-diffusion of seismicity despite the driving mechanism (see the discussion in Ref.[36]).

The msd of seismicity for periods B1 and B2 are shown in Fig. 5a and b, respectively, in an event-by-event calculation. During the first 6 days of earthquake activity during period B1, the mean distance of seismicity is decreasing, showing stronger clustering closer to the reference point (1st event) rather than migrating away, as it would be expected in a diffusion process.

After the surpass of the first six days, we fit the msd of seismicity with Eq. (5), which shows an approximate power-law growth with time with a diffusion exponent $a = 0.054 \pm 0.007$ (Fig. 5a), indicating a very weak sub-diffusive process. For period B2, an active diffusion mechanism becomes more apparent. During the first three days of activity, seismicity migrates rapidly away from the "source", which coincides with the systematic shallowing of the relocated earthquake depths (Fig. 2). This migration becomes slower after the third day and approximates the power-law growth with time (Eq. (5)), with a diffusion exponent of $a = 0.294 \pm 0.011$ (Fig. 5b), indicating a slow sub-diffusive process.
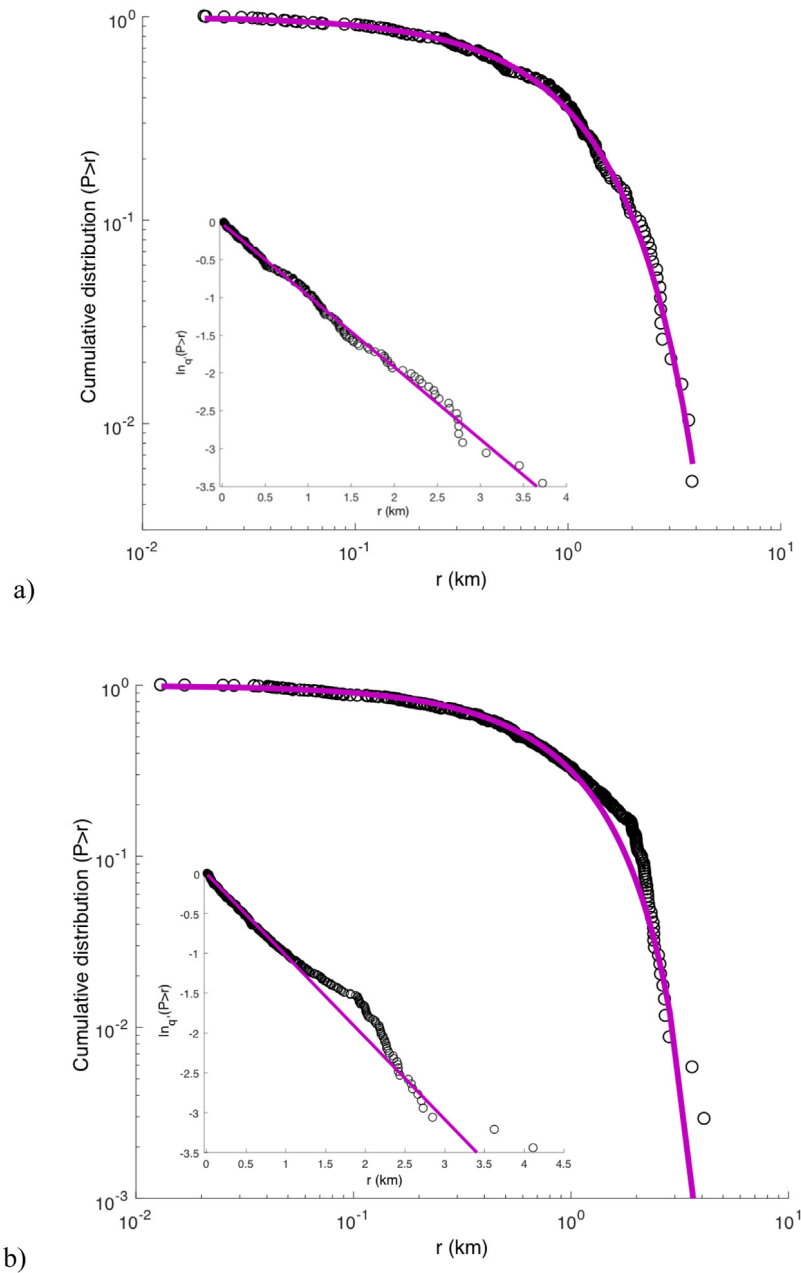
Fig. 4. (a) Cumulative distribution function $P(>r)$ of the inter-event distances r for period B1 and the corresponding fit according to the q-exponential distribution (Eq. (2)) for the values of $q_r = 0.87$ and $r_0 = 1.13$ (solid line). Inset: the corresponding q-logarithmic distribution that approximates linearity with the correlation coefficient of -0.998. (b) The same for period B2. The solid line indicates the q-exponential distribution for the values of $q_r = 0.75$ and $r_0 = 1.215$, while in the inset the corresponding q-logarithmic distribution is shown that approximates linearity with the correlation coefficient of -0.992.

4. Discussion

In the present work we studied the physical characteristics of micro-seismicity that occurred during 2012–2014 near the CO_2-rich Florina basin and its possible connection with an active diffusion mechanism. We have seen that micro-seismicity started to occur sporadically on July 2012 on the northern cluster (cluster A), while the southern cluster (cluster B) was mainly activated at the end of July 2013 after the installation of the local network, although it is not clear whether this cluster was active prior to that period with small magnitude earthquakes that were not detected by the regional permanent network.

We further focused on the earthquake activity that occurred after the installation of the local network at the end of July

2013, which provided a more comprehensive image of the activated fault structures and the evolution of micro-seismicity in the area. Essentially, we focused on cluster B, where the great majority of earthquakes occurred during this time period. Furthermore, our focus on cluster B offered the opportunity to study the earthquake characteristics on a single fault structure rather than on a regional fault network. The available dataset shows that micro-seismicity on cluster B mainly occurred within two distinct periods of activity (periods B1–B2) that lasted approximately 66 and 49 days, respectively. During those two periods, cluster B was repeatedly activated within smaller clusters of events with an almost vertical alignment of events with depth. In one such case at the beginning of period B2, earthquake events started to occur in deeper parts ($\sim$4 km) and then were migrating towards the surface ($\sim$2 km), indicating a diffusive process. The similar
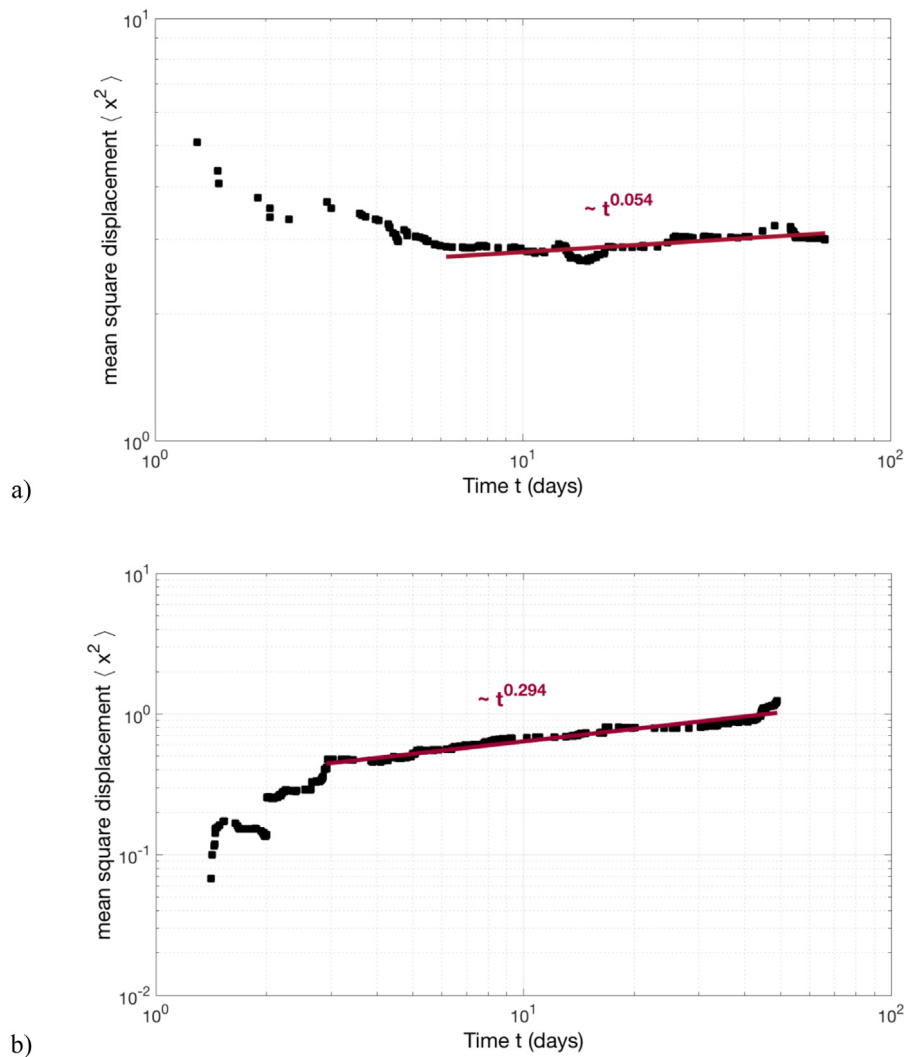
Fig. 5. Mean square displacement $\langle x^2(t) \rangle$ of seismicity (squares) with time t in double logarithmic axes, for (a) period B1 and (b) period B2. The solid lines indicate the power-law growth of $\langle x^2(t) \rangle$ according to Eq. (5) after the surpass of (a) six days and (b) three days.

waveforms of the recorded earthquakes and the similar locations along cluster B found by Ref. 5, indicate that a similar mechanism was responsible for earthquake triggering along the active fault plane.

We studied the spatiotemporal scaling properties of micro-seismicity in cluster B, for earthquakes with magnitude $M \geq Mc$, during the two periods (B1–B2) to find possible organization patterns and correlations in the spatiotemporal evolution of seismicity. The analysis showed that the cumulative distribution of inter-event times $P(>\tau)$ between successive events can well be approximated with the q-exponential distribution, with similar q_τ-values ($q_\tau \approx 1.5$) for the two periods, indicating a similar temporal structure of seismicity during the two periods of activation of cluster B. The q_τ-values well above unity indicate asymptotic power-law behavior, long-range correlations between the events and organization, rather than random (Poissonian) behavior, in the temporal evolution of seismicity.[32]

Furthermore, the quality of the relocated catalog and the small location errors (2 – 35 m) offered the opportunity to also study the spatial scaling properties of micro-seismicity. As for $P(>\tau)$, the cumulative distributions of inter-event distances $P(>r)$ can well be approximated with the q-exponential distribution, but in this case with q_r-values less than unity, showing organization rather than random spatial occurrence of events, similar to the

results of previous studies.[28,31,32] Spatial organization in this case can be related with a fractal structure of breaking asperities along the active fault plane. The different q_r-values found for the two periods of activation ($q_r = 0.87$ for period B1 and $q_r = 0.75$ for period B2) may reflect the volume of activation. During period B1 the majority of events was comprised inside a $\sim$2.5 km area occurring irregularly on the structure[5] showing a q_r-value closer to unity and a distribution closer to random behavior (exponential), whereas during period B2 seismicity initiated on a $\sim$3 km area and systematically progressed towards the entire activated structure showing a lower q_r-value. This progression of seismicity towards the entire structure might also be the reason for the deviation of $P(>r)$ from the q-exponential distribution at inter-event distances around $\sim$1.5 – 2 km (Fig. 4b), where slightly higher probabilities to encounter successive earthquakes at these inter-event distances, than those predicted from the model, are observed.

In addition, we studied the diffusion properties of micro-seismicity along cluster B during the two periods (B1–B2) of activation by estimating the mean square displacement (msd) of seismicity with time in respect to the 1st event ("reference"). During period B1, no, or particularly after the surpass of 6 days, very weak diffusion is observed. This is not the case for period B2, where earthquake diffusion according to a sub-diffusive process

is clearly observed. During the first three days of period B2, the diffusion of seismicity is even faster, associated with the migration of events towards shallower depths, as it was earlier discussed. The diffusion exponent ($a \approx 0.3$) well below unity that marks normal diffusion in homogeneous and isotropic media, indicates the anomalous diffusion of seismicity. Such result is in accordance with a fluid diffusion mechanism along the activated fault structure.[36] In such case, anomalous diffusion of seismicity due to fluid flow can be related to structure heterogeneities and anisotropic diffusivities due to strong spatial variability of the permeability field.[36]

The almost vertical alignment with depth observed within smaller clusters of events in cluster B, the migration of seismicity towards shallower depths observed in one of these cases, as well as the slow diffusion of seismicity found for one of the activation periods of cluster B (period B2), suggest the involvement of fluid diffusion in the triggering mechanism of micro-seismicity in the area. Pressurized fluids, in this case, can be related to CO_2 migration that is moving towards the surface in the CO_2-rich Florina basin. Increased CO_2 emissions following earthquake swarms have been observed in the western Eger rift[41] and the Mammoth Mountain.[42] Unfortunately, in our case there are no recordings of CO_2 emissions in the surface during that period, or the period following right after, that could further support this hypothesis. Additional triggering mechanisms, however, such as event–event triggering and/or static stress transfer from the $M_w 4.1$ earthquake that occurred on 17 February 2013 on cluster A, cannot be excluded, highlighting the complexity of the process. Mesimeri et al.[5] showed that cluster B lies within positive Coulomb stress changes caused by the occurrence of the $M_w 4.1$ earthquake, with $\Delta\text{CFF} > 0.01$ MPa in some of the lobes, which can be considered adequate for triggering new events. A plausible scenario in this case can be that positive stress transfer due to the occurrence of the $M_w 4.1$ earthquake could have triggered the micro-seismic activity that was observed during period B1 on cluster B, in which very weak earthquake diffusion is observed. This result is in accordance to previous results that have shown low diffusion exponents and weak sub-diffusion associated with stress diffusion and/or a cascade of triggering/triggered earthquakes.[39,40] In addition, the breaking of asperities during period B1 could have modified permeability along the fault zone, further favoring CO_2 upwelling, which could then have triggered micro-seismicity during period B2 that presents clear characteristics of earthquake diffusion and a larger diffusion exponent, with a value similar to another case of episodic micro-seismicity associated with fluid diffusion at depth.[36]

5. Conclusions

In the present work we have studied the scaling and diffusion properties of micro-seismicity that occurred during 2012–2014 in the SW margin of the CO_2-rich Florina basin. The spatial distribution of micro-seismicity in the area defines two clusters, one dipping to the north (cluster A), which includes the largest event of the sequence ($M_w 4.1$), and the other gently dipping to the south having an almost vertical alignment (cluster B). Focusing on cluster B that was mainly activated after the installation of a local network in the area, we find spatiotemporal organization patterns and correlations during both periods of activation (periods B1–B2) that contradict the random (Poissonian) occurrence of events. In addition, by estimating the mean square displacement of the sequence, we find that no or very weak diffusion is observed during the first period of activation (period B1), while during the second period (period B2) earthquake diffusion becomes apparent, following a slow sub-diffusive process.

Earthquake diffusion during the second period (period B2) of activation along cluster B, the almost vertical alignment of

events with depth, as well as the migration of seismicity towards shallower depths observed in one of the smaller clusters within cluster B, suggest the involvement of fluid diffusion in the triggering mechanism of micro-seismicity in the area. However, secondary triggering mechanisms due to stress transfer cannot be excluded, emphasizing the complexity of the process that does not permit to uniquely define the processes leading to seismicity. The continued surveillance and monitoring of seismicity and CO_2 discharging in the CO_2-rich Florina basin would be quite useful for better constraining the mechanics of the seismically active hydrothermal system and the relation between seismicity and CO_2 emissions. This is quite important for better estimating the associated earthquake and environmental hazards, particularly in areas that are considered as natural analogues for carbon geological storage as the Florina basin.

Declaration of competing interest

Acknowledgments

References

1. Roman DC, Cashman KV. The origin of volcano-tectonic earthquake swarms. *Geology*. 2006;34(6):457–460. http://dx.doi.org/10.1130/G22269.1.
2. Fischer T, Horálek J, Hrubcová P, Vavryčuk V, Bräuer K, Kämpf H. Intra-continental earthquake swarms in west-bohemia and vogtland: a review. *Tectonophysics*. 2014;611:1–27. http://dx.doi.org/10.1016/j.tecto.2013.11.001.
3. Shelly DR, Hill DP. Migrating swarms of brittle-failure earthquakes in the lower crust beneath Mammoth Mountain, California. *Geophys Res Lett*. 2011;38:L20307. http://dx.doi.org/10.1029/2011GL049336.
4. Hainzl S, Fischer T. Indications for a successively triggered rupture growth underlying the 2000 earthquake swarm in Vogtland/NW Bohemia. *J Geophys Res Solid Earth*. 2002;107(B12). http://dx.doi.org/10.1029/2002jb001865, ESE-5.
5. Mesimeri M, Karakostas V, Papadimitriou E, Tsaklidis G, Tsapanos T. Detailed microseismicity study in the area of Florina (Greece) Evidence for fluid driven seismicity. *Tectonophysics*. 2017;694:424–435. http://dx.doi.org/10.1016/j.tecto.2016.11.027.
6. Lewicki JL, Hilley GE, Shelly DR, King JC, McGeehin JP, Mangan M, Evans WC. Crustal migration of CO_2-rich magmatic fluids recorded by tree-ring radiocarbon and seismicity at Mammoth Mountain, CA, USA. *Earth Planet Sci Lett*. 2014;390:52–58. http://dx.doi.org/10.1016/j.epsl.2013.12.035.
7. Parotidis M, Shapiro SA, Rothert E. Evidence for triggering of the vogtland swarms 2000 by pore pressure diffusion. *J Geophys Res B*. 2005;110:1–12. http://dx.doi.org/10.1029/2004JB003267.
8. Miller SA, Collettini C, Chiaraluce L, Cocco M, Barchi M, Kaus BJP. Aftershocks driven by a high-pressure CO_2 source at depth. *Nature*. 2004;427:724–727. http://dx.doi.org/10.1038/nature02251.
9. Shapiro SA, Rothert E, Rath V, Rindschwentner J. Characterization of fluid transport properties of reservoirs using induced microseismicity. *Geophysics*. 2002;67(1):212–220. http://dx.doi.org/10.1190/1.1451597.
10. Heinicke J, Fischer T, Gaupp R, Götze J, Koch U, Konietzky H, Stanek KP. Hydrothermal alteration as a trigger mechanism for earthquake swarms: the Vogtland/NW Bohemia region as a case study. *Geophys J Int*. 2009;178(1):1–13. http://dx.doi.org/10.1111/j.1365-246X.2009.04138.x.
11. Ziogou F, Gemeni V, Koukouzas N, de Angelis D, Libertini S, Beaubien SE, Lombardi S, West JM, Jones DG, Coombs P, Barlow TS, Gwosdz S, Krüger M. Potential environmental impacts of CO_2 leakage from the study of natural analogue sites in Europe. *Energy Procedia*. 2013;37:1–8. http://dx.doi.org/10.1016/j.egypro.2013.06.245.

12. D'Alessandro W, Bellomo S, Brusca L, Karakazanis S, Kyriakopoulos K, Liotta M. The impact on water quality of the high carbon dioxide contents of the groundwater in the area of Florina (N. Greece). In: Lambrakis N, Stournaras G, Katsanou K, eds. *Advances in the Research of Aquatic Environment*. Environmental Earth Sciences, Springer; 2011, p. 135–143.

13. Koukouzas N, Tasianas A, Gemeni V, Alexopoulos D, Vasilatos C. Geological modelling for investigating CO2 emissions in Florina basin, Greece. *Open Geosci*. 2015;7(2015):465–489. http://dx.doi.org/10.1515/geo-2015-0039.

14. Koukouzas N, Ziogou F, Gemeni V. Preliminary assessment of CO_2 geological storage opportunities in Greece. *Int J Greenhouse Gas Control*. 2009;3:502–513. http://dx.doi.org/10.1016/j.ijggc.2008.10.005.

15. Papazachos BC, Papazachou C. *The Earthquakes of Greece*. Ziti publications: Thessaloniki; 2003.

16. Jaynes ET. Information theory and statistical mechanics. *Phys Rev*. 1957;106:620–630.

17. Tsallis C. Possible generalization of Boltzmann–Gibbs Statistics. *J Stat Phys*. 1988;52:479–487.

18. Tsallis C. *Introduction to Nonextensive Statistical Mechanics: Approaching a Complex World*. Springer: Berlin; 2009.

19. Main I. Statistical physics, seismogenesis, and seismic hazard. *Rev Geophys*. 1996;34:433–462.

20. Turcotte DL. *Fractals and Chaos in Geology and Geophysics*. 2nd ed., Cambridge University Press: Cambridge, UK; 1997.

21. Michas G, Vallianatos F, Sammonds P. Non-extensivity and long-range correlations in the earthquake activity at the West Corinth rift (Greece). *Nonlinear Process Geophys*. 2013;20:713–724. http://dx.doi.org/10.5194/npg-20-713-2013.

22. Michas G, Sammonds P, Vallianatos F. Dynamic multifractality in earthquake time series: Insights from the Corinth rift, Greece. *Pure Appl Geophys*. 2015;172:1909–1921.

23. Michas G, Vallianatos F. Stochastic modeling of nonstationary earthquake time series with long-term clustering effects. *Phys Rev E*. 2018;98:042107. http://dx.doi.org/10.1103/PhysRevE.98.042107.

24. Picoli S, Mendes RS, Malacarne LC, Santos RPB. Q- distributions in complex systems: A brief review. *Braz J Phys*. 2009;39:468–474. http://dx.doi.org/10.1590/S0103-97332009000400023.

25. Vallianatos F, Sammonds P. A non-extensive statistics of the fault-population at the valles marineris extensional province, Mars. *Tectonophys*. 2011;509:50–54. http://dx.doi.org/10.1016/j.23tecto.2011.06.001.

26. Vallianatos F, Michas G, Papadakis G. A description of seismicity based on non-extensive statistical physics: A review. In: S. D'Amico, ed. *Earthquakes and their Impact on Society*. Springer; 2016, p. 1–41. http://dx.doi.org/10.1007/978-3-319-21753-6.

27. Michas G, Vallianatos F, Sammonds P. Statistical mechanics and scaling of fault populations with increasing strain in the Corinth Rift. *Earth Planet Sci Lett*. 2015;431:150–163.

28. Abe S, Suzuki N. Law for the distance between successive earthquakes. *J Geophys Res*. 2003;108:2113.

29. Caruso F, Pluchino A, Latora V, Vinciguerra S, Rapisarda A. Analysis of self-organized criticality in the Olami-Feder-Christensen model and in real earthquakes. *Phys Rev E*. 2007;75:055101.

30. Telesca L. Analysis of Italian seismicity by using a nonextensive approach. *Tectonophysics*. 2010;494:155–162.

31. Papadakis G, Vallianatos F, Sammonds P. Evidence of nonextensive statistical physics behavior of the Hellenic Subduction Zone seismicity. *Tectonophysics*. 2013;608:1037–1048.

32. Vallianatos F, Papadakis G, Michas G. Generalized statistical mechanics approaches to earthquakes and tectonics. *Proc R Soc Lond Ser A Math Phys Eng Sci*. 2016;472:20160497. http://dx.doi.org/10.1098/rspa.2016.0497.

33. Efstathiou A, Tzanis A, Vallianatos F. On the nature and dynamics of the seismogenetic systems of north California, USA: An analysis based on Non-Extensive Statistical Physics. *Phys Earth Planet Inter*. 2017;270:46–72. http://dx.doi.org/10.1016/j.pepi.2017.06.010.

34. Vallianatos F, Michas G, Papadakis G. Nonextensive statistical seismology: An overview. In: Chelidze T, Vallianatos F, Telesca L, eds. *Complexity of Seismic Time Series*. Elsevier; 2018, p. 25–59. http://dx.doi.org/10.1016/B978-0-12-813138-1.00002-X.

35. Seber G, Wild C. *Non-Linear Regression*. Wiley: New York; 1989.

36. Michas G, Vallianatos F. Modelling earthquake diffusion as a continuous-time random walk with fractional kinetics: The case of the 2001 Agios Ioannis earthquake swarm (Corinth Rift). *Geophys J Int*. 2018. http://dx.doi.org/10.1093/gji/ggy282.

37. Bouchaud JP, Georges A. Anomalous diffusion in disordered media: statistical mechanisms, models and physical applications. *Phys Rep*. 1990;195:127–293. http://dx.doi.org/10.1016/0370-1573(90)90099-N.

38. Marsan D, Bean CJ, Steacy S, McCloskey J. Observation of diffusion processes in earthquake populations and implications for the predictability of seismicity systems. *J Geophys Res*. 2000;105:28081–28094.

39. Helmstetter A, Ouillon G, Sornette D. Are aftershocks of large California earthquakes diffusing?. *J Geophys Res*. 2003;108. ESE9–1-ESE9-24.

40. Huc M, Main IG. Anomalous stress diffusion in earthquake triggering: correlation length, time dependence, and directionality. *J Geophys Res*. 2003;108:2324.

41. Bräuer K, Kämpf H, Strauch G, Weise SM. Isotopic evidence (^{3}He/^{4}He,^{13}C$_{CO2}$) of fluid-triggered intraplate seismicity. *J Geophys Res*. 2003;108(B2):2070. http://dx.doi.org/10.1029/2002JB002077.

42. Werner C, Bergfeld D, Farrar CD, Doukas MP, Kelly PJ, Kern C. Decadal-scale variability of diffuse CO_2 emissions and seismicity revealed from long-term monitoring (1995–2013) at Mammoth Mountain, California, USA. *J Volcanol Geotherm Res*. 1995;289(2014):51–63. http://dx.doi.org/10.1016/j.jvolgeores.2014.10.020.

43. Wessel P, Smith WHF. New improved version of the generic mapping tools released. *EOS Trans Am Geophys Union*. 1998;79:579. http://dx.doi.org/10.1029/98EO00426.